Materials Chemistry and Physics 216 (2018) 413–420

Contents lists available at ScienceDirect

Materials Chemistry and Physics

journal homepage: www.elsevier.com/locate/matchemphys

Pseudocapacitive response of hydrothermally grown MoS_2 crumpled nanosheet on carbon fiber

Kush K. Upadhyay[a,*], Tuyen Nguyen[a], Teresa M. Silva[a,b], Maria J. Carmezim[a,c], M.F. Montemor[a]

[a] Centro de Química Estructural-CQE, Departamento de Engenharia Química, Instituto Superior Técnico, Universidade de Lisboa, 1049-001, Lisboa, Portugal
[b] Department of Mechanical Engineering, GI-MOSM, Instituto Superior de Engenharia de Lisboa - ISEL, 1950-062, Lisboa, Portugal
[c] ESTSetúbal, Instituto Politécnico de Setúbal, 1959-007, Setúbal, Portugal

HIGHLIGHTS

- MoS_2 crumpled nanosheet synthesized directly on carbon fiber paper by hydrothermal synthesis.
- The synthesized material delivered the specific capacitance of 249 F g^{-1} at 2 A g^{-1}
- It retained 41.3% of initial capacitance at 10 A g^{-1}
- EIS showed very low ESR and very short relaxation time ~0.36 s.

ARTICLE INFO

Keywords:
MoS_2 crumpled nanosheet
Supercapacitors
Hydrothermal synthesis
Negative electrode
Short relaxation time

ABSTRACT

Crumpled MoS_2 nanosheets were synthesized directly on carbon fiber paper (CFP) through hydrothermal procedure. Molybdenum sulfide precursor was first produced in the solution and then introduced into the autoclave. Scanning electron microscopy (SEM) and transmission electron microscopy (TEM) images confirmed the uniform growth of crumpled nanosheets on the CFP that were assigned to MoS_2 according to X-ray photo electron spectroscopy (XPS) and Raman spectroscopy results. Electrochemical measurements of the as deposited MoS_2 crumpled nanosheets performed in 1 M Na_2SO_4 evidenced a specific capacitance of 249 F g^{-1} at 2 A g^{-1} and the good rate capability by retaining 41.3% of initial capacitance at 10 A g^{-1}. Electrochemical Impedance spectroscopy measurements showed very low charge transfer resistance and very short relaxation time accounting for the pseudocapacitive rectangular cyclic voltammetry (CV) and high rate capability.

1. Introduction

2D transition metal dichalcogenides, like MoS_2, WS_2, WSe_2, and $MoSe_2$, have drawn considerable attention because of their layered structure, similar to graphene [1–4], and owing to several properties such as electronic, optical, and catalytic activity [5–8]. Among them, MoS_2 has been extensively studied for various applications, namely dye-sensitized solar cell, supercapacitors, Li-ion batteries, hydrogen evolution reaction, sensors amongst others [9–12].

Molybdenum sulfides usually consist of a mixture of two major polytypes of similar structure: a trigonal prismatic phase, labelled as 2H, space group D_{3h} and an octahedral one, labelled 1T, space group O_h. The 2H phase is relatively stable, but its conductivity is low when compared to the 1T phase, which is metastable and, due to its metallic character, presents high conductivity [13–15]. MoS_2 layered structure is based on a hexagonal crystal in which Mo atom is six-fold coordinated and hexagonally packed between two trigonally co-ordinated sulphur atoms making S-Mo-S layers. These packed layers are stacked together by weak Van der Waals interaction [16,17], which allow for easy intercalation of cations throughout all available surface [18]. Also, MoS_2 possess higher intrinsic ionic conductivity than oxides and almost three and half times higher specific capacity than that of commercially available graphite anodes (372 mA h g^{-1}) [19,20]. The high charge transportation ability of MoS_2, combined with a large specific surface area, because of its 2D layered structure, are crucial factors for enhanced electrochemical response and application as supercapacitor electrodes. Moreover, charge storage in layered MoS_2 happens through different ways, which include intersheet double layer formation, facilitated by available open structure, intrasheet double layer charge storage on individual atomic MoS_2 layers via diffusion into the basal edges, and faradaic charge transfer process occurring on Mo metal centres, which are known for exhibiting multiple valence states

* Corresponding author.
E-mail address: kush.upadhyay@tecnico.ulisboa.pt (K.K. Upadhyay).

https://doi.org/10.1016/j.matchemphys.2018.06.029
Received 12 August 2017; Received in revised form 13 April 2018; Accepted 11 June 2018
Available online 11 June 2018
0254-0584/

ranging from +2 to +6 and rich chemistry [19,21,22].

Various synthesis routes have been developed for synthesizing MoS_2 and its composites including chemical vapour deposition (CVD) [19], mechanical and chemical exfoliation [15,23–26], hydrothermal [27–32], magnetron sputtering [33], electrodeposition and electrochemical anodization [34,35], microwave assisted growth [36] and solution based synthesis [20,37]. However, there are very few reports on the direct synthesis of layered molybdenum sulfide on carbon-based surfaces. Kien-Cuong Pham et al. electrodeposited MoS_2 on graphene carbon nanotube/carbon paper substrate in two step process; in the first one graphene carbon nanotube hybrids were grown by CVD approach and molybdenum sulfide was deposited on top of grown graphene carbon nanotube hybrid on carbon paper in the second step. The overall hybrid system showed specific capacitance of 414 F g^{-1} at 0.67 A g^{-1} versus 140 F g^{-1} at 0.67 A g^{-1}, obtained for MoS_2 deposited on carbon paper [34]. Krishnamoorthy et al. sulfurized molybdenum foil using thiourea as the sulphur source and the directly grown MoS_2 displayed a specific capacitance of 192.7 F g^{-1} at 1 mA cm^{-2} [32]. Recently Lina Wang [31] reported specific capacitances of 133 F g^{-1} at 1 A g^{-1} for MoS_2 grown on titanium plate substrates.

In this work MoS_2 crumpled nanosheets were synthesized directly on carbon fibre paper by a hydrothermal route. The CFP substrate was chosen because of its advantageous properties such as high conductivity, light weight and chemical inertness towards the electrolyte [38,39]. This strategy eliminates the complex fabrication process of supercapacitor electrodes, which normally includes making a slurry, by mixing conducting carbon and binders with the active material, pasting, drying etc. Moreover, this route that avoids the need of binders increases the electrode conductivity and eliminates de-adhesion failures. The synthesized material showed specific capacitance of 249 F g^{-1} at 2 A g^{-1} with good rate capability.

2. Experimental

2.1. MoS_2 synthesis

The precursors taken for MoS_2 synthesis were sodium molybdate dihydrate ($Na_2MoO_4.2H_2O$) sodium sulphide (Na_2S) and sulfuric acid (H_2SO_4). These chemicals were used as received without any further purification.

Na_2MoO_4 (Mo source) and Na_2S (sulphur source) were dissolved in deionized water under vigorous stirring for 45 min to achieve concentrations of 0.03 M and 0.12 M, respectively. The obtained electrolyte, containing MoO_4^{2-} and excess of S^{2-} ions presented a pH of 12.3. Before hydrothermal synthesis, conversion of molybdate to thiomolybdate was done in solution using 1 M H_2SO_4. On adding slowly, the acid to the electrolyte, a change in the color from colourless to yellow was observed, associated with the release of H_2S gas and, when pH dropped to ~8.5, the development of deep brown color was observed. On further addition of the acidic solution the pH reached 7, and the evolution of H_2S gas increased significantly inducing simultaneous conversion of MoO_4^{2-} to MoS_4^{2-} according to reaction (1):

$$MoO_4^{2-} + 6S^{2-} + 12H^+ \leftrightarrow MoS_4^{2-} + 4H_2\,O + 2H_2S\uparrow \quad (1)$$

The thiomolybdate solution was then transferred to an autoclave for hydrothermal synthesis leading to the formation of MoS_2 [40].

Carbon fiber paper (Toray®), used as substrate, supported with glass slide dipped into the solution at some inclination to the teflon liner to avoid the contact of carbon fiber paper to the teflon liner. The initial mass of the CFP substrate was measured carefully before dipping into the solution. The area of the substrate exposed to the electrolyte was 1 × 1 cm^2. Afterwards the autoclave was sealed properly and kept into oven at 180 °C for 12 h. After normal cooling of the autoclave, the substrate, with the deposited material on the exposed area, was rinsed with DI water several times and kept for drying at room temperature for 24 h. After the proper dry, final mass of the substrate + deposit was measured carefully.

2.1.1. Materials characterization

Surface morphology of the CFP substrate and of the deposited material was investigated by field emission scanning electron microscopy (FEG-SEM, JEOL 7001F) connected with energy dispersive spectrometer (EDS) for elemental mapping. To assess further structural information, transmission electron microscopy (TEM) was also performed using a Hitachi H8100 200 kV microscope with thermionic emission gun (LaB6), equipped with EDS, allowing elemental analysis of the synthesized material. To avoid any change in the structure, sample preparation was done with proper care. Some part of the sample was scratched and the resulting powder was taken on the grid directly for the investigation.

Phase and structural analysis of the deposited films was performed by X-ray diffraction (XRD) using a Bruker AXS D8 Advance diffractometer having Cu Kα radiation of 1.5418 Å. Vibrational modes of the bonds of hydrothermally deposited samples were characterized by Raman spectroscopy in the range of interest from 350 cm^{-1} to 430 cm^{-1}.

XPS analysis was carried out to find out the chemical composition and the corresponding oxidation states of the deposited material. XPS spectra were acquired in constant analyser energy (CAE) mode (30 eV), using an Al (non-monochromatic) anode and an accelerating voltage of 15 kV. Deconvolution of the XPS spectra was performed using Avantage software and all spectra were referred to C 1s binding energy (284.7 eV).

2.1.2. Electrochemical characterization

The electrochemical behaviour of the synthesized MoS_2 films were evaluated by cyclic voltammetry (CV), at scan rates ranging from 10 to 200 mV s^{-1} and by galvanostatic charge-discharge measurement (GCD) at varying current densities (ranging from 2 to 10 A g^{-1}) in 1 M Na_2SO_4 solution, using PGZ 100 potentiostat. Bare CFP was also investigated by CV for comparison. Both CV and GCD were measured in the potential window of −0.4 V to 0.25 V. Electrochemical impedance spectroscopy (EIS) was performed to study the resistive response of fresh and cycled sample. The experiments were carried out using a Gamry Femtostat, at the OCP, applying a sinusoidal perturbation with 10 mV of amplitude (RMS) and frequencies ranging from 50 kHz to 5 mHz.

All electrochemical measurements were performed in three electrode set-up where platinum was used as counter electrode, standard calomel electrode (SCE) as reference electrode and the deposited material as working electrode.

3. Results and discussion

3.1. Physico chemical characterization

The surface morphology of bare CFP and deposited material on its top is depicted in Fig. 1. In the case of bare substrate (Fig. 1a) it can be clearly seen that CFP fibers, presenting a thickness in the range of 5–7 μm, are interconnected well to each other, contributing to the good electronic conductivity of the substrate. It can also be observed that the entangle CFP results into wide voids, which is expected to facilitate diffusion of electrolyte. Fig. 1b shows the SEM image of hydrothermally synthesized material, at low magnification, showing that the deposition of material occurred uniformly all around the CFP fibers as evidenced in the magnified image shown in the inset of Fig. 1b. In the SEM image shown in Fig. 1c, the morphology of crumpled nanosheets is evidenced as well as the uniform coverage of the CFP. Further analysis at a nanometric scale demonstrated that the crumpled nanosheets are very thin and that the crumpled morphology results in the formation of wide holes as evidenced in Fig. 1d. These morphological features could result in increased surface area, enabling the accessibility of electrolyte to a

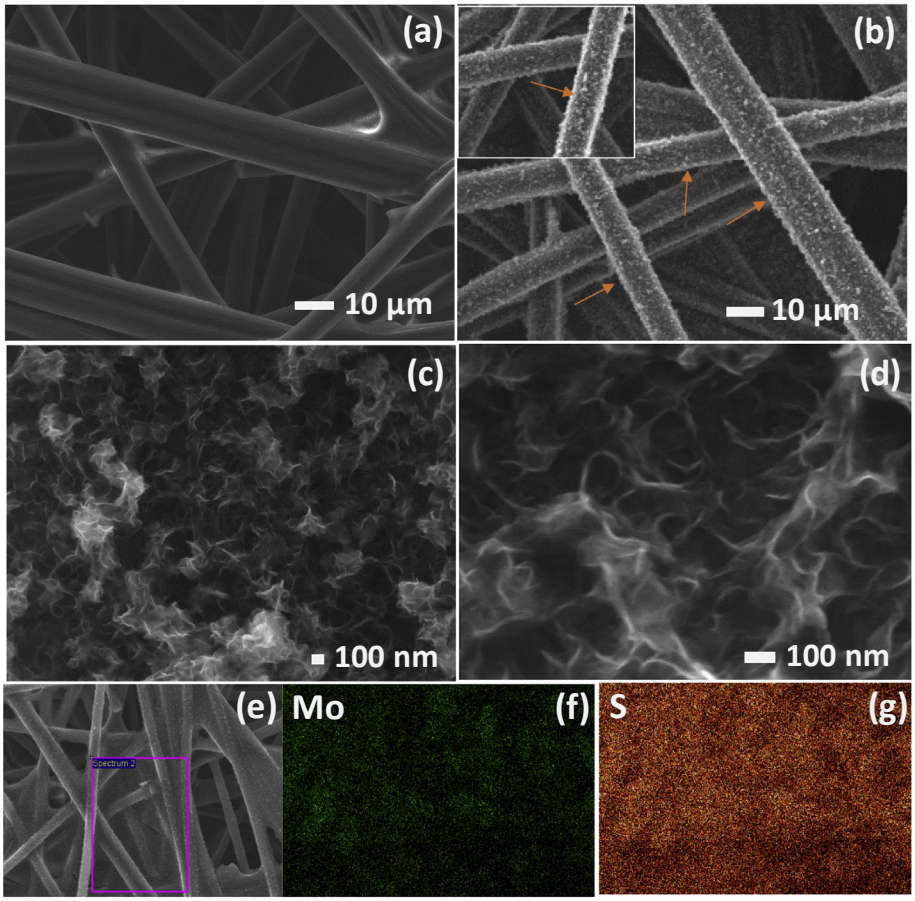

Fig. 1. SEM image of bare CFP (a); MoS_2 on CFP at different magnifications (b–d), EDS mapping in selected area (e-g).

larger area of the active material. EDS mapping performed at selected area, Fig. 1e–g, evidenced uniform distribution of Mo and S that covered the CFP substrate.

To detail the structural morphology, TEM analysis was performed - Fig. 2. The results confirmed the previous SEM observations and evidenced the growth of thin crumpled nanosheets uniformly over the CFP fibers – Fig. 2a. The images at higher magnification (Fig. 2 b and c) illustrate the formation of a very thin crumpled nanosheet structure, having thickness in the range of ~10 nm illustrated in Fig. 2c. The EDS perfromed attached to TEM again confirmed the presence of Mo and S in the deposited film (Fig. 2d).

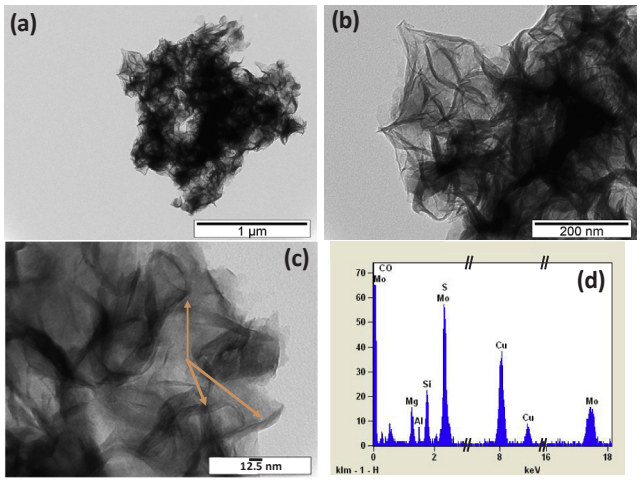

Fig. 2. TEM images (a–c); and EDS spectra of MoS_2 (d).

XRD measurements were recorded for phase analysis by varying the 2Θ value from 10 to 80° (Fig. 3a). The deposited material corresponded to the 2H-MoS_2 hexagonal structure, with sharp peaks at 2Θ values of 14.75°, 32.44°, 35.86°, 44.1° and 58.2°, which can be assigned to (002), (100), (102), (006) and (110) lattice planes, respectively. These peaks are in good agreement with JCPDS card number-037-1492 and previous reports [41,42]. Sharp peaks and absence of undesired reflections indicated the good crystallinity and purity of the as prepared material.

Raman spectroscopy was employed to confirm the atomic structural arrangement of MoS_2. As shown in Fig. 3b, two characteristic Raman active modes, E^1_{2g} and A_{1g}, can be observed at 379.6 cm^{-1} and 404.8 cm^{-1}, respectively. The assigned peaks matched well with previous report for MoS_2 nanosheets synthesized at pH 7 [41]. The in plane E^1_{2g} mode originates from opposite vibration of two S atoms with respect to the Mo atom, while A_{1g} mode arises from out of plane vibration of only S atoms in opposite directions [43]. The peak position of A_{1g} mode directly relates to the thickness of MoS_2 nanosheets; in fact, the observed A_{1g} Raman mode at 404.8 cm^{-1} was red shifted compared to the bulk MoS_2 Raman peak, which generally originates at 408 cm^{-1}, suggesting the formation of few-layered MoS_2 nanosheets [32,43].

The chemical state of MoS_2 was studied from X-ray photoelectron spectroscopy (XPS). Fig. 3 (c) shows the high resolution XPS scan in Mo 3d, which is partially overlapped with the S 2s region. The deconvulated peaks, having the binding energy of 232.51 eV and 229.21 eV can be assigned to +4 oxidation state of Mo $3d_{3/2}$ and $3d_{5/2}$ in MoS_2, respectively [44–46]. Also the relatively low intense doublet at 236.11 eV and 233.01 eV corresponds to +6 oxidation state of Mo $3d_{3/2}$ and $3d_{5/2}$, respectively [47,48]; the peaks at 234.41 eV and 229.81 eV also corresponds to +6 oxidation state of Mo $3d_{3/2}$ and $3d_{5/2}$. According to

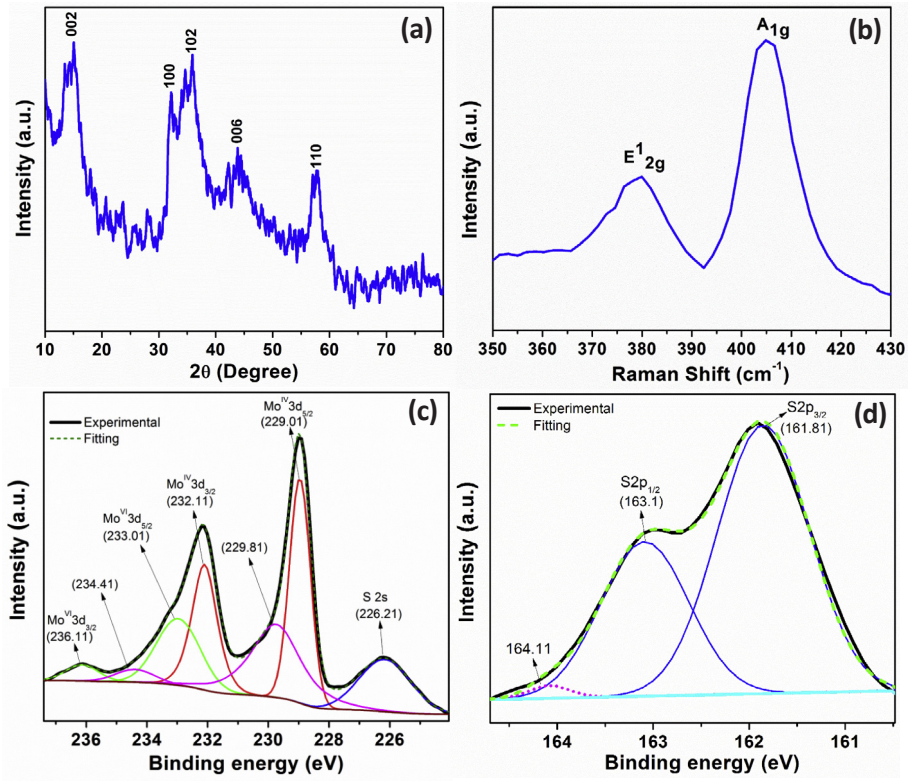

Fig. 3. XRD (a), Raman (b) and XPS spectra of Mo 3d-S 2s regions (c) and S 2p regions (d) of MoS_2.

previous reports, the emergence of such +6 oxidation state may be related to the formation of MoO_xS_y species, such as $MoO_{1.0}S_{2.0}$ [49,50]. The presence of oxides and oxysulfides peaks could be because of partial air oxidation of the MoS_2 surface [44]. The peak at 226.11 eV corresponds to S 2s and confirms the presence of Sulphur [34]. The S2p doublet in Fig. 3d, was deconvulated into 2 peaks, one located at 163.1 eV and another at 161.81 eV that correspond to apical S^{2-} or bridging S_2^{2-} and basal plane S^{2-} or terminal S_2^{2-} respectively [45]. The small peak at 164.11 eV is from elemental sulphur [51]. The XPS results suggest that the Mo^{4+} and S^{2-} were the dominant states in the deposited material.

The capacitive behaviour of the deposited sample was examined by cyclic voltammetry and galvanostatic charge discharge measurements as depicted in Fig. 4. The CV of bare CFP performed at 50 mV s^{-1} is also included for comparative purposes. It showed negligible current response, indicating that the current response is due to MoS_2. The CV profiles for MoS_2 measured at different scan rates (Fig. 4a) evidenced, in all cases, a rectangular shape similar to the carbon-based materials response, confirming the nearly ideal capacitive behaviour of the material in this potential window. The absence of redox peaks indicate that the current response is originated either from double layer formation or from the occurrence of multiple surface successive reversible redox reactions at the electrode/electrolyte interface, which involves substoichiometric variation in the electrode material due to electro-adsorption of proton or cations known as pseudocapacitance [52]. Based on literature, the two possible mechanisms (double layer formation and faradaic processes) responsible for charge storage are described below [19].

In case of double layer formation, protons or cations (in this case Na^+) denoted as C^+ are adsorbed on the surface of nanosheets (equation (2)), according to:

$$(MoS_2)_{surface} + C^+ (H^+ \text{ or } Na^+) + e^- \leftrightarrow (MoS_2 - C^+)_{surface} \quad (2)$$

and, in the case of fast reversible faradaic process, protons or alkali cations may diffuse into the interlayer of MoS_2 structure [19], according to equation (3):

$$MoS_2 + C^+ (H^+ \text{ or } Na^+) + e^- \leftrightarrow (MoS - SC^+) \quad (3)$$

Moreover, the increase in the anodic and cathodic current intensity with the scan rate, as observed from the CV profiles, confirms the reversible electrochemical behaviour of the deposited material and its good capacitive behaviour even at very high scan rates (200 mV s^{-1}). This can be associated with the open structure of the material (attained because of the crumpled nanosheets), which reduces diffusion control at high scan rates.

Galvanostatic charge-discharge measurements were performed at different current densities to calculate the specific capacitance, rate capability and capacitance retention of the deposited material. As shown in Fig. 4b, the linear profile of the charge-discharge curve evidences the typical double layer and/or pseudocapacitive behaviour, which is in agreement with the voltammetric response. The specific capacitance of the material was calculated from the charge-discharge data by using equation (4):

$$C_s = \frac{I\,\Delta t}{\Delta V} \quad (4)$$

where, C_s is the specific capacitance (F g^{-1}), I is the current density (A g^{-1}), Δt is the discharge time (s) and ΔV is the working potential window. The specific capacitance values calculated for the different current density are depicted in Fig. 4c. A maximum specific capacitance of 249 F g^{-1} was obtained at current density of 2 A g^{-1}. Moreover, the deposited material showed good rate capability by retaining a specific capacitance of 103 F g^{-1} at 10 A g^{-1} which is 41.3% of initial capacitance.

To meet practical requirements, the cyclic stability of the material is of prime importance. Galvanostatic charge-discharge measurements were performed over 1000 cycles to acquire this information. The results are presented in Fig. 4d and evidenced a retention of 71% of the initial capacitance after 1000 cycles.

Compared to data form literature (Table 1), the directly grown MoS_2

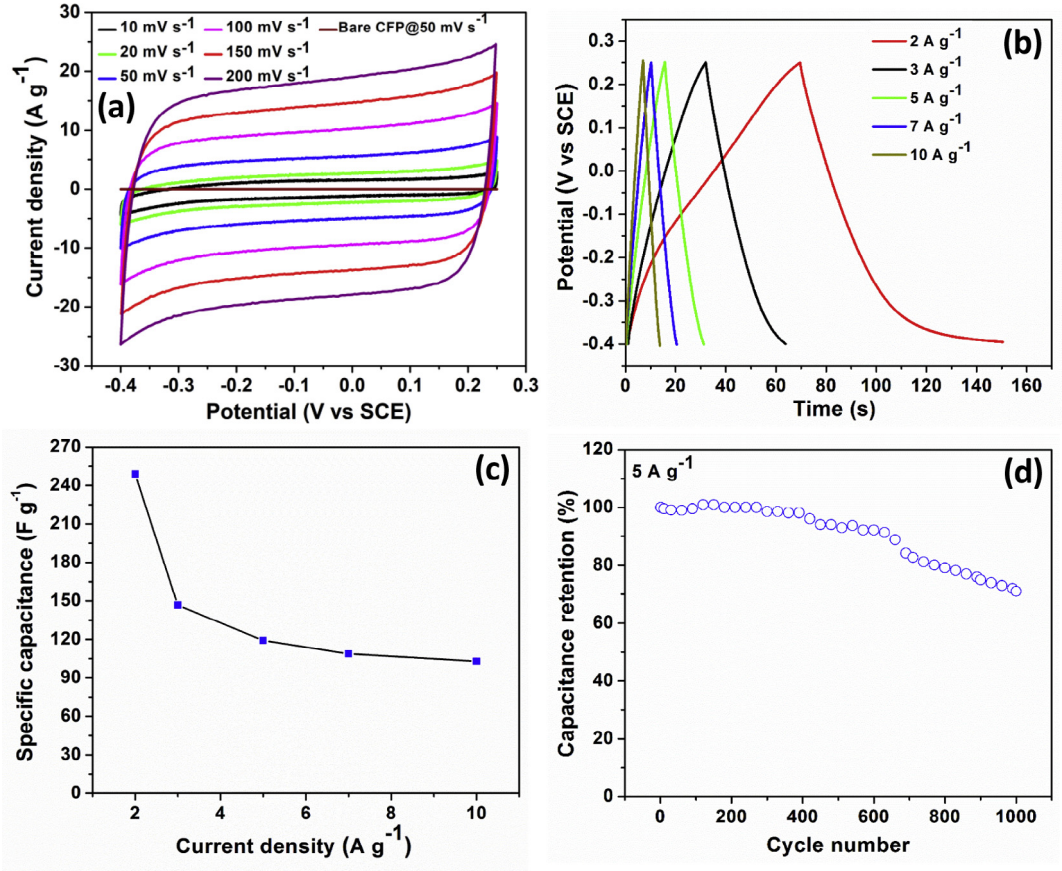

Fig. 4. Cyclic voltammetry of deposited MoS_2 at different scan rate (including the bare CFP performed at 50 mV s^{-1}) (a), galvanostatic charge-discharge measurement at different current densities (b), specific capacitance *vs.* current density (c) and stability up to 1000 cycles (d).

crumpled nanosheets on carbon fibres proposed in this work shows enhanced electrochemical response as charge storage material. The good specific capacitance, reasonable capacity fade and, particularly, the good rate capability can be related to the morphology of the crumpled nanosheets and their good connection with the CFP substrate, which facilitates charge storage, reduces diffusion controlled processes and ensures good electronic conductivity.

To characterize further the deposited materials, electrochemical impedance spectroscopy (EIS) was carried out at the open circuit potential for the MoS_2 films before and after applying 1000 potential cycles (aged material). The spectra are shown in Fig. 5, along with the equivalent circuit proposed to fit the data, and the fitted values of the material before cycling presented in Table 2.

The Nyquist plot gives information about the charge transfer resistance at high frequency and capacitive behaviour at low frequency. The absence of a semi-circle in the high frequency region, as can be noticed from magnified plot shown in inset of Fig. 5a, and the very low value of 0.002 Ω cm^2 obtained from fitting (Table 2) suggest negligible charge transfer resistance.

CPE_{dl} is the constant phase element representing the double layer capacitance, which specifically occurs at the electrode/electrolyte interface due to the separation of ionic and electronic charges. In the high frequency region most of the capacitance generally arises from the double layer formation. The admittance of the CPE_{dl} obtained by fitting was 1.1 μF cm^{-2} $s^{\alpha-1}$, being consistent with previous reports [59,60].

The emergence of Warburg behaviour denoted by W_o in the mid frequency region represents the frequency dependent diffusion of ions. A well-defined and short Warburg region portion, with phase angle of around −45° (n = 0.55), evidences the short and equal diffusion path length of the ions in the electrolyte. Also the Warburg resistance value

Table 1
Synthesis procedure, specific capacitance and stability comparison of some previous reports.

Material	Synthesis procedure	Directly on substrate	Specific Capacitance	Stability	Reference
MoS_2 nanosheet	Hydrothermal	No	129.2 F g^{-1} at 1 A g^{-1}	85.1% after 500 cycles	[53]
Flower like MoS_2 nanostructure	Hydrothermal	No	159 F g^{-1} at 2 A g^{-}	92.6% after 3000 cycles	[29]
MoS_2 Sphere	Hydrothermal	No	92.85 F g^{-1} at 0.5 mA cm^{-2}	93.8% after 1000 cycles	[54]
MoS_2 nanostructure	Hydrothermal	No	122 F g^{-1} at 0.5 A g^{-1}	Not mentioned	[55]
3D-tubular MoS_2	Hydrothermal	No	276 F g^{-1} at 0.5 A g^{-1}	96% after 1000 cycles	[56]
MoS_2 nanosheet	Ball milling-mechanical exfoliation	No	89.02 F g^{-1} at 5 mV s^{-1}	89.36% after 2500 cycles	[57]
MoS_2 nanoflowers	Hydrothermal	No	169 F g^{-1} at 1 A g^{-1}	85.3% after 3000 cycles	[58]
MoS_2 film	Magnetron sputtering	Yes	33 mF cm^{-2} at 25.47 mA cm^{-2}	97% after 5000 cycles	[33]
MoS_2 nanosheet	Hydrothermal sulfurization of Mo substrate	Yes	192.7 F g^{-1} at 1 mA g^{-1}	98% after 1000 cycles	[32]
MoS_2 on titanium plate	Hydrothermal	Yes	133 F g^{-1} at 1 A g^{-1}	93% after 1000 cycles	[31]
MoS_x on carbon paper	Electrodeposition	Yes	140 F g^{-1} at 0.67 A g^{-1}	Not mentioned	[34]
MoS2 crumpled nanosheet	Hydrothermal	Yes	249 F g^{-1} at 2 A g^{-1}	71% after 1000 cycles	This work

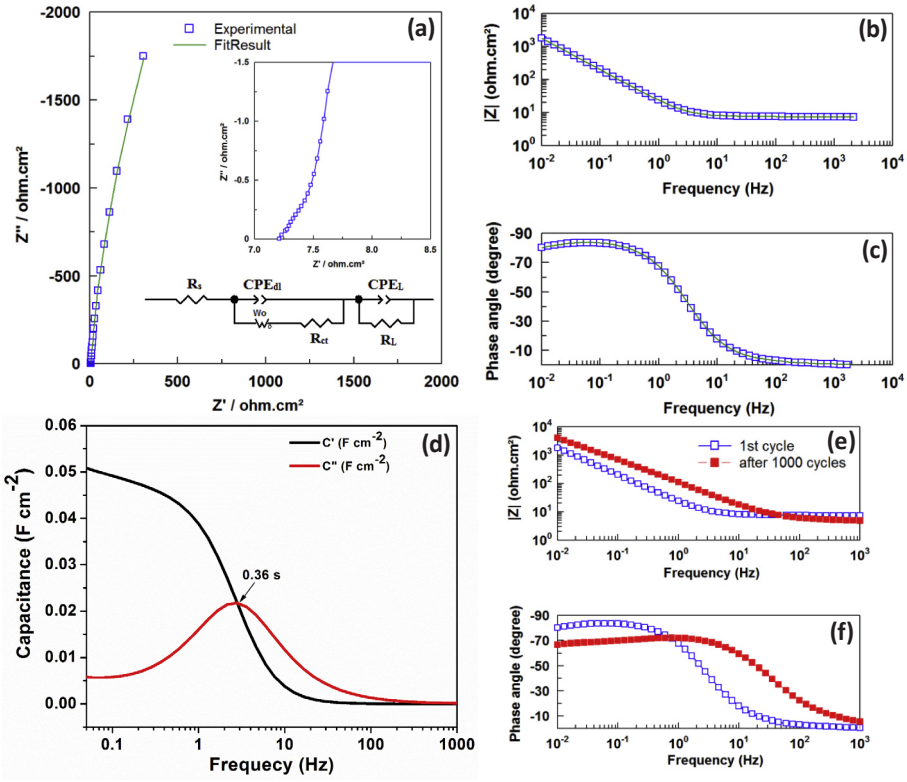

Fig. 5. Electrochemical Impedance spectroscopy (EIS) of deposited material; Nyquist plot (a) (inset showing the magnified image and equivalent circuit diagram, green line is the fitted curve of experimental data), Bode plots (b, c); evolution of real part and imaginary capacitance *vs.* frequency (d), Bode plots comparing the material after 1 cycle and after 1000 cycles (e, f).

Table 2
Electrochemical impedance parameters obtained after fitting the experimental data for the fresh sample before cycling.

Fitting parameters		Value
R_s ($\Omega.cm^2$)		7.21
R_{ct} ($\Omega.cm^2$)		0.002
CPE_{dl}($\mu F.cm^{-2}s^{\alpha-1}$)		1.1
Warburg element,W_o	($\Omega.cm^2$)	0.94
	n	0.55
n (at low frequency)		
Rl($\Omega.cm^2$)		15.9
CPE_L($\mu F.cm^{-2}s^{\alpha-1}$)		0.88
χ^2 Value		$7.4 * 10^{-5}$

of 0.94 $\Omega\,cm^2$ was very low. The very low charge transfer resistance and the decreased diffusion effect can be the reason for very fast reversible redox reactions at the interface, which explains the rectangular CV, the rectangular nature retention even at high scan rates and the linear profiles of GCD plots.

At very low frequency, the capacitance generally originates from the reversible redox process (pseudocapacitance) represented as CPE_L in the equivalent circuit. The admittance of CPE_L, 15.9 $\mu F\,cm^{-2}\,s^{\alpha-1}$, was obtained after fitting the EIS spectra, being significantly higher than the CPE_{dl} value obtained at higher frequencies. This was an expected result since at low frequencies ions have sufficient time to diffuse throughout the deposited film, which increases the active area available for the redox processes. R_L is the leakage resistance connected in parallel to the CPE_L and its value, presented in Table 2, is 6164 $\Omega\,cm^2$ which is significantly high. Low leakage resistances imply high leakage currents that induces fast electrode discharge. The high leakage resistance obtained for the deposited material points to low self-discharge tendency. Also, the marked vertical curve having a n value of 0.88 and phase angle around −84° (Fig. 5c), in the low frequency region, indicates an almost ideal supercapacitor response [59,60].

EIS data has been used to study in detail the supercapacitive behaviour of similar materials. Taberna et al. [61] have done a detailed study on the capacitive and impeding behaviour of carbon based materials from EIS data. The complex formulation for capacitance dependent on frequency is defined as:

$$C(\omega) = C'(\omega) + C''(\omega) \quad (5)$$

Where

$$C'(\omega) = \frac{-Z''(\omega)}{\omega|Z(\omega)|^2} \quad (6)$$

$$C''(\omega) = \frac{Z'(\omega)}{\omega\,|Z(\omega)|^2} \quad (7)$$

and

$$Z(\omega) = Z'(\omega) + Z''(\omega) \quad (8)$$

Where C′(ω) and C"(ω) are the real and imaginary part of the complex capacitance, respectively and Z′(ω) and Z"(ω) are the frequency dependent real and imaginary part of the impedance, respectively. The C′(ω) and C"(ω) *vs* frequency of the deposited material is illustrated in Fig. 5d.

In terms of physical meaning, the value of C′(ω) corresponds to the capacitance of the electrode and depends on the electrode structure and electrode/electrolyte interface. As it can be seen from the plot in Fig. 5d, in the high frequency region the material displays poor capacitive behaviour meaning it behaves as resistor. As frequency goes down, and when it reaches approximately 20 Hz, a sudden increase in the capacitance can be noticed. For low frequencies capacitance undergoes saturation after attaining a maximum. This behaviour can be explained considering that at high frequencies electrolyte ions can only have the access to the surface of the deposited material, whereas the material inside deeper pores is not accessed. In contrast, at low frequencies, electrolyte ions have sufficient time to penetrate deep inside the pores of the film accessing more electrode surface thereby contributing to the high capacitance value.

C"(ω) corresponds to the energy dissipation by an irreversible

process that can lead to a hysteresis, which also can be stated as dielectric loss of the electrolyte ions due to rotation or movement of molecules dependent on frequency. The variation of C"(ω) *vs.* frequency is presented in Fig. 5d. The plot displays a maximum at particular frequency f_0. This frequency corresponds to dielectric relaxation time, given by $t_0 = 1/f_0$, and represents the supercapacitor factor of merit [61]. The relaxation time calculated for the deposited material is 0.36 s and this value indicates the minimum time needed to discharge all the energy of the device with an efficiency higher than 50%. The short relaxation time obtained for crumpled nanosheets MoS_2 accounts for the short diffusional path of ions and efficient charge-discharge ability and is nearly in the same range, or even shorter, compared to other reported materials such as activated carbon (0.7 s) [62], dried self-stacked solvated graphene (0.43 s) [63], vertically oriented graphene grown on nickel foam current collector (0.36 s) [64], MWCNT (0.7 s) or AC (1 s) [65].

Impedance analysis was also performed after 1000 GCD cycles and compared to the measurement on the as prepared material. The substantial increase in the resistance, particularly in low-mid frequency region, and lowering of phase angle in the same frequency range, observed from the spectra presented in Fig. 5e and f provides an explanation for the cyclic degradation of the deposited material, possibly because of dissolution or formation of non-reversible species.

4. Conclusions

In summary, MoS_2 crumpled nanosheets were synthesized directly on carbon fiber paper by hydrothermal procedure for supercapacitor application. The material covered the entire carbon fiber surface and XPS results suggested that Mo^{4+} and S^{2-} were the dominant states in the deposited material. MoS_2 crumpled nanosheets showed very good pseudocapacitive behaviour, attaining specific capacitance of 249 F g^{-1} at 2 A g^{-1} with a good rate capability. MoS_2 crumpled nanosheets also retained around 71% of initial capacitance after 1000 cycles. Electrochemical impedance spectroscopy showed short relaxation time of 0.36 s making it a promising electrode material for high power applications.

Acknowledgements

All authors would like to thank Fundação para a Ciência e a Tecnologia for the funding under the contract UID/QUI/00100/2013, M-ERA-NET/0004/2014 and RECI/QEQ-QIN/0189/2012. K.K. Upadhyay would like to acknowledge Erasmus Mundus NAMASTE (20130674) for funding.

References

[1] A.K. Geim, K.S. Novoselov, The rise of graphene, Nat. Mater. 6 (2007) 183–191.
[2] C.N.R. Rao, A.K. Sood, Graphene: Synthesis, Properties, and Phenomena, Wiley-VCH, Verlag GmbH, Weinheim, 2013.
[3] X. Liu, J.-Z. Zhang, K.-J. Huang, P. Hao, Net-like molybdenum selenide–acetylene black supported on Ni foam for high-performance supercapacitor electrodes and hydrogen evolution reaction, Chem. Eng. J. 302 (2016) 437–445.
[4] Y.-P. Gao, X. Wu, K.-J. Huang, L.-L. Xing, Y.-Y. Zhang, L. Liu, Two-dimensional transition metal diseleniums for energy storage application: a review of recent developments, CrystEngComm 19 (2017) 404–418.
[5] S. Ratha, C.S. Rout, Supercapacitor electrodes based on layered tungsten disulfide-reduced graphene oxide hybrids synthesized by a facile hydrothermal method, ACS Appl. Mater. Interfaces 5 (2013) 11427–11433.
[6] M.-R. Gao, Y.-F. Xu, J. Jiang, S.-H. Yu, Nanostructured metal chalcogenides: synthesis, modification, and applications in energy conversion and storage devices, Chem. Soc. Rev. 42 (2013) 2986–3017.
[7] G. Cunningham, M. Lotya, C.S. Cucinotta, S. Sanvito, S.D. Bergin, R. Menzel, M.S.P. Shaffer, J.N. Coleman, Solvent exfoliation of transition metal dichalcogenides: dispersibility of exfoliated nanosheets varies only weakly between compounds, ACS Nano 6 (2012) 3468–3480.
[8] J.N. Coleman, M. Lotya, A. O'Neill, S.D. Bergin, P.J. King, U. Khan, K. Young, A. Gaucher, S. De, R.J. Smith, I.V. Shvets, S.K. Arora, G. Stanton, H.-Y. Kim, K. Lee, G.T. Kim, G.S. Duesberg, T. Hallam, J.J. Boland, J.J. Wang, J.F. Donegan, J.C. Grunlan, G. Moriarty, A. Shmeliov, R.J. Nicholls, J.M. Perkins, E.M. Grieveson, K. Theuwissen, D.W. McComb, P.D. Nellist, V. Nicolosi, Two-Dimensional nanosheets produced by liquid exfoliation of layered materials, Science 331 (2011) 568–571.
[9] J. Theerthagiri, R.A. Senthil, B. Senthilkumar, A. Reddy Polu, J. Madhavan, M. Ashokkumar, Recent advances in MoS_2 nanostructured materials for energy and environmental applications – a review, J. Solid State Chem. 252 (2017) 43–71.
[10] G. Zhang, H. Liu, J. Qu, J. Li, Two-dimensional layered MoS_2: rational design, properties and electrochemical applications, Energy Environ. Sci. 9 (2016) 1190–1209.
[11] W.-J. Zhang, K.-J. Huang, A review of recent progress in molybdenum disulfide-based supercapacitors and batteries, Inorganic Chemistry Frontiers 4 (2017) 1602–1620.
[12] Y.-H. Wang, K.-J. Huang, X. Wu, Recent advances in transition-metal dichalcogenides based electrochemical biosensors: a review, Biosens. Bioelectron. 97 (2017) 305–316.
[13] T. Wang, L. Liu, Z. Zhu, P. Papakonstantinou, J. Hu, H. Liu, M. Li, Enhanced electrocatalytic activity for hydrogen evolution reaction from self-assembled monodispersed molybdenum sulfide nanoparticles on an Au electrode, Energy Environ. Sci. 6 (2013) 625–633.
[14] D. Voiry, H. Yamaguchi, J. Li, R. Silva, D.C.B. Alves, T. Fujita, M. Chen, T. Asefa, V.B. Shenoy, G. Eda, M. Chhowalla, Enhanced catalytic activity in strained chemically exfoliated WS_2 nanosheets for hydrogen evolution, Nat. Mater. 12 (2013) 850–855.
[15] M. Acerce, D. Voiry, M. Chhowalla, Metallic 1T phase MoS_2 nanosheets as supercapacitor electrode materials, Nat. Nanotechnol. 10 (2015) 313–318.
[16] A.K. Geim, I.V. Grigorieva, Van der Waals heterostructures, Nature 499 (2013) 419–425.
[17] J. Brivio, D.T.L. Alexander, A. Kis, Ripples and layers in ultrathin MoS_2 membranes, Nano Lett. 11 (2011) 5148–5153.
[18] RadenovicA. RadisavljevicB, GiacomettiV. BrivioJ, KisA, single-layer MoS_2 transistors, Nat. Nanotechnol. 6 (2011) 147–150.
[19] J.M. Soon, K.P. Loh, Electrochemical double-layer capacitance of MoS_2 nanowall films, Electrochem. Solid State Lett. 10 (2007) A250–A254.
[20] K. Chang, W. Chen, In situ synthesis of MoS_2/graphene nanosheet composites with extraordinarily high electrochemical performance for lithium ion batteries, Chem. Commun. 47 (2011) 4252–4254.
[21] X. Hu, W. Zhang, X. Liu, Y. Mei, Y. Huang, Nanostructured Mo-based electrode materials for electrochemical energy storage, Chem. Soc. Rev. 44 (2015) 2376–2404.
[22] K.K. Upadhyay, T. Nguyen, T.M. Silva, M.J. Carmezim, M.F. Montemor, Electrodeposited MoO_x films as negative electrode materials for redox supercapacitors, Electrochim. Acta 225 (2017) 19–28.
[23] H.S.S. Ramakrishna Matte, A. Gomathi, A.K. Manna, D.J. Late, R. Datta, S.K. Pati, C.N.R. Rao, MoS_2 and WS_2 analogues of graphene, Angew. Chem. Int. Ed. 49 (2010) 4059–4062.
[24] K.-G. Zhou, N.-N. Mao, H.-X. Wang, Y. Peng, H.-L. Zhang, A mixed-solvent strategy for efficient exfoliation of inorganic graphene analogues, Angew. Chem. Int. Ed. 50 (2011) 10839–10842.
[25] M.B. Sadan, L. Houben, A.N. Enyashin, G. Seifert, R. Tenne, Atom by atom: HRTEM insights into inorganic nanotubes and fullerene-like structures, Proc. Natl. Acad. Sci. Unit. States Am. 105 (2008) 15643–15648.
[26] M.A. Bissett, I.A. Kinloch, R.A.W. Dryfe, Characterization of MoS_2–graphene composites for high-performance coin cell supercapacitors, ACS Appl. Mater. Interfaces 7 (2015) 17388–17398.
[27] X. Zhou, B. Xu, Z. Lin, D. Shu, L. Ma, Hydrothermal synthesis of flower-like MoS_2 nanospheres for electrochemical supercapacitors, J. Nanosci. Nanotechnol. 14 (2014) 7250–7254.
[28] A. Ramadoss, T. Kim, G.-S. Kim, S.J. Kim, Enhanced activity of a hydrothermally synthesized mesoporous MoS_2 nanostructure for high performance supercapacitor applications, N. J. Chem. 38 (2014) 2379–2385.
[29] X. Wang, J. Ding, S. Yao, X. Wu, Q. Feng, Z. Wang, B. Geng, High supercapacitor and adsorption behaviors of flower-like MoS_2 nanostructures, J. Mater. Chem. 2 (2014) 15958–15963.
[30] M. Wang, H. Fei, P. Zhang, L. Yin, Hierarchically layered MoS_2/Mn_3O_4 hybrid architectures for electrochemical supercapacitors with enhanced performance, Electrochim. Acta 209 (2016) 389–398.
[31] L. Wang, Y. Ma, M. Yang, Y. Qi, Titanium plate supported MoS_2 nanosheet arrays for supercapacitor application, Appl. Surf. Sci. 396 (2017) 1466–1471.
[32] K. Krishnamoorthy, G.K. Veerasubramani, P. Pazhamalai, S.J. Kim, Designing two dimensional nanoarchitectured MoS_2 sheets grown on Mo foil as a binder free electrode for supercapacitors, Electrochim. Acta 190 (2016) 305–312.
[33] N. Choudhary, M. Patel, Y.-H. Ho, N.B. Dahotre, W. Lee, J.Y. Hwang, W. Choi, Directly deposited MoS_2 thin film electrodes for high performance supercapacitors, J. Mater. Chem. 3 (2015) 24049–24054.
[34] K.-C. Pham, D.S. McPhail, A.T.S. Wee, D.H.C. Chua, Amorphous molybdenum sulfide on graphene-carbon nanotube hybrids as supercapacitor electrode materials, RSC Adv. 7 (2017) 6856–6864.
[35] Y. Yang, H. Fei, G. Ruan, C. Xiang, J.M. Tour, Edge-oriented MoS2 nanoporous films as flexible electrodes for hydrogen evolution reactions and supercapacitor devices, Adv. Mater. 26 (2014) 8163–8168.
[36] E.G. da Silveira Firmiano, A.C. Rabelo, C.J. Dalmaschio, A.N. Pinheiro, E.C. Pereira, W.H. Schreiner, E.R. Leite, Supercapacitor electrodes obtained by directly bonding 2D MoS_2 on reduced graphene oxide, Advanced Energy Materials 4 (2014) 1301380-n/a.
[37] C. Altavilla, M. Sarno, P. Ciambelli, A novel wet chemistry approach for the synthesis of hybrid 2D free-floating single or multilayer nanosheets of MS_2@

oleylamine (M=Mo, W), Chem. Mater. 23 (2011) 3879–3885.
[38] L. Huang, D. Chen, Y. Ding, S. Feng, Z.L. Wang, M. Liu, Nickel–cobalt hydroxide nanosheets coated on $NiCo_2O_4$ nanowires grown on carbon fiber paper for high-performance pseudocapacitors, Nano Lett. 13 (2013) 3135–3139.
[39] K.K. Upadhyay, S. Eugénio, R. Della Noce, T.M. Silva, M.J. Carmezim, M.F. Montemor, Hydrothermally grown $Ni_{0.7}Zn_{0.3}O$ directly on carbon fiber paper substrate as an electrode material for energy storage applications, Int. J. Hydrogen Energy 41 (2016) 9876–9884.
[40] E.A. Ponomarev, M. Neumann-Spallart, G. Hodes, C. Lévy-Clément, Electrochemical deposition of MoS_2 thin films by reduction of tetrathiomolybdate, Thin Solid Films 280 (1996) 86–89.
[41] L. Yang, X. Cui, J. Zhang, K. Wang, M. Shen, S. Zeng, S.A. Dayeh, L. Feng, B. Xiang, Lattice strain effects on the optical properties of MoS_2 nanosheets, Sci. Rep. 4 (2014) 5649.
[42] A.K. Thakur, R.B. Choudhary, M. Majumder, G. Gupta, M.V. Shelke, Enhanced electrochemical performance of polypyrrole coated MoS_2 nanocomposites as electrode material for supercapacitor application, J. Electroanal. Chem. 782 (2016) 278–287.
[43] H. Li, Q. Zhang, C.C.R. Yap, B.K. Tay, T.H.T. Edwin, A. Olivier, D. Baillargeat, From bulk to monolayer MoS_2: evolution of Raman scattering, Adv. Funct. Mater. 22 (2012) 1385–1390.
[44] J. Kibsgaard, Z. Chen, B.N. Reinecke, T.F. Jaramillo, Engineering the surface structure of MoS_2 to preferentially expose active edge sites for electrocatalysis, Nat. Mater. 11 (2012) 963–969.
[45] T. Weber, J.C. Muijsers, J.W. Niemantsverdriet, Structure of amorphous MoS_3, J. Phys. Chem. 99 (1995) 9194–9200.
[46] G. Eda, H. Yamaguchi, D. Voiry, T. Fujita, M. Chen, M. Chhowalla, Photoluminescence from chemically exfoliated MoS_2, Nano Lett. 11 (2011) 5111–5116.
[47] M.R. Smith, U.S. Ozkan, The partial oxidation of methane to formaldehyde: role of different crystal planes of MoO_3, J. Catal. 141 (1993) 124–139.
[48] V.I. Nefedov, M.N. Firsov, I.S. Shaplygin, Electronic structures of $MRhO_2$, MRh_2O_4, $RhMO_4$ and Rh_2MO_6 on the basis of X-ray spectroscopy and ESCA data, J. Electron. Spectrosc. Relat. Phenom. 26 (1982) 65–78.
[49] L. Benoist, D. Gonbeau, G. Pfister-Guillouzo, E. Schmidt, G. Meunier, A. Levasseur, X-ray photoelectron spectroscopy characterization of amorphous molybdenum oxysulfide thin films, Thin Solid Films 258 (1995) 110–114.
[50] L. Benoist, D. Gonbeau, G. Pfister-Guillouzo, E. Schmidt, G. Meunier, A. Levasseur, XPS analysis of lithium intercalation in thin films of molybdenum oxysulphides, Surf. Interface Anal. 22 (1994) 206–210.
[51] D. Brion, Etude par spectroscopie de photoelectrons de la degradation superficielle de FeS2, $CuFeS_2$, ZnS et PbS a l'air et dans l'eau, Appl. Surf. Sci. 5 (1980) 133–152.
[52] G.Z. Chen, Supercapacitor and supercapattery as emerging electrochemical energy stores, Int. Mater. Rev. 62 (2017) 173–202.
[53] K.-J. Huang, J.-Z. Zhang, G.-W. Shi, Y.-M. Liu, Hydrothermal synthesis of molybdenum disulfide nanosheets as supercapacitors electrode material, Electrochim. Acta 132 (2014) 397–403.
[54] K. Krishnamoorthy, G.K. Veerasubramani, S. Radhakrishnan, S.J. Kim, Supercapacitive properties of hydrothermally synthesized sphere like MoS_2 nanostructures, Mater. Res. Bull. 50 (2014) 499–502.
[55] P. Ilanchezhiyan, G. Mohan Kumar, T.W. Kang, Electrochemical studies of spherically clustered MoS_2 nanostructures for electrode applications, J. Alloy. Comp. 634 (2015) 104–108.
[56] L. Ren, G. Zhang, Z. Yan, L. Kang, H. Xu, F. Shi, Z. Lei, Z.-H. Liu, Three-Dimensional tubular MoS_2/PANI hybrid electrode for high rate performance supercapacitor, ACS Appl. Mater. Interfaces 7 (2015) 28294–28302.
[57] K. Krishnamoorthy, P. Pazhamalai, G.K. Veerasubramani, S.J. Kim, Mechanically delaminated few layered MoS_2 nanosheets based high performance wire type solid-state symmetric supercapacitors, J. Power Sources 321 (2016) 112–119.
[58] X. Cui, X. Chen, S. Chen, F. Jia, S. Yang, Z. Lin, Z. Shi, H. Deng, Dopamine adsorption precursor enables N-doped carbon sheathing of MoS_2 nanoflowers for all-around enhancement of supercapacitor performance, J. Alloy. Comp. 693 (2017) 955–963.
[59] W. Wang, S. Guo, I. Lee, K. Ahmed, J. Zhong, Z. Favors, F. Zaera, M. Ozkan, C.S. Ozkan, Hydrous ruthenium oxide nanoparticles anchored to graphene and carbon nanotube hybrid foam for supercapacitors, Sci. Rep. 4 (2014) 4452.
[60] C. Masarapu, H.F. Zeng, K.H. Hung, B. Wei, Effect of temperature on the capacitance of carbon nanotube supercapacitors, ACS Nano 3 (2009) 2199–2206.
[61] P.L. Taberna, P. Simon, J.F. Fauvarque, Electrochemical characteristics and impedance spectroscopy studies of carbon-carbon supercapacitors, J. Electrochem. Soc. 150 (2003) A292–A300.
[62] D. Pech, M. Brunet, H. Durou, P. Huang, V. Mochalin, Y. Gogotsi, P.-L. Taberna, P. Simon, Ultrahigh-power micrometre-sized supercapacitors based on onion-like carbon, Nat. Nanotechnol. 5 (2010) 651–654.
[63] X. Yang, J. Zhu, L. Qiu, D. Li, Bioinspired effective prevention of restacking in multilayered graphene films: towards the next generation of high-performance supercapacitors, Adv. Mater. 23 (2011) 2833–2838.
[64] Z. Bo, W. Zhu, W. Ma, Z. Wen, X. Shuai, J. Chen, J. Yan, Z. Wang, K. Cen, X. Feng, Vertically oriented graphene bridging active-layer/current-collector interface for ultrahigh rate supercapacitors, Adv. Mater. 25 (2013) 5799–5806.
[65] C. Portet, G. Yushin, Y. Gogotsi, Electrochemical performance of carbon onions, nanodiamonds, carbon black and multiwalled nanotubes in electrical double layer capacitors, Carbon 45 (2007) 2511–2518.